Title: The influence of impact direction and axial loading on the bone fracture pattern

Authors: Haim Cohen, Chen Kugel, Hila May, Bahaa Medlej, Dan Stein, Viviane Slon, Tamar Brosh, Israel Hershkovitz

PII: S0379-0738(17)30186-X
DOI: http://dx.doi.org/doi:10.1016/j.forsciint.2017.05.015
Reference: FSI 8853

To appear in: *FSI*

Received date: 17-6-2016
Revised date: 19-1-2017
Accepted date: 13-5-2017

Please cite this article as: Haim Cohen, Chen Kugel, Hila May, Bahaa Medlej, Dan Stein, Viviane Slon, Tamar Brosh, Israel Hershkovitz, The influence of impact direction and axial loading on the bone fracture pattern, Forensic Science Internationalhttp://dx.doi.org/10.1016/j.forsciint.2017.05.015

Complete manuscript title: The influence of impact direction and axial loading on the bone fracture pattern

Haim Cohen [a, b*] haimcoh1@post.tau.ac.il

Chen Kugel [b ,c] chen.kugel@forensic.health.gov.il

Hila May [a] hilamay@gmail.com

Bahaa Medlej [a] Bahaamedlej@gmail.com

Dan Stein [a] maadan@gmail.com

Viviane Slon [a, e] slonviviane@gmail.com

Tamar Brosh [d] tbrosh@post.tau.ac.il

Israel Hershkovitz [a] anatom2@post.tau.ac.il

[a] Department of Anatomy and Anthropology, Sackler Faculty of Medicine, Tel Aviv University, Tel Aviv 69978, Israel

[b] National Center of Forensic Medicine,Tel Aviv 61490, Israel

[c] Sackler Faculty of Medicine, Tel Aviv University, Tel Aviv 69978, Israel

[d] Laboratory of Fine Measurements, Dental School of Medicine, Tel-Aviv University, Israel

[e] Department of Evolutionary Genetics, Max Planck Institute for Evolutionary Anthropology, 04103 Leipzig, Germany.

Grant sponsors: Dan David Foundation, Tassia and Dr. Joseph Meychan Chair for the History and Philosophy of Medicine.

*Correspondence: Dr. Haim Cohen, Department of Anatomy and Anthropology, Sackler Faculty of Medicine, Tel Aviv University, Tel Aviv 69978, Israel

Tel: 972-3-6409495; Fax: 972-3-6408287; E-mail: haimcoh1@post.tau.ac.il

Highlights

- We examined the influence of impact direction and axial loading on the bone fracture pattern.
- Five different tests in different directions and loading situations were carried out.
- The impact direction and the presence of axial loading during impact significantly affected the fracture pattern.
- None of our experiments (with and without compression) yielded a "true" butterfly fracture.

Abstract

The effect of the direction of the impact and the presence of axial loading on fracture patterns have not yet been established in experimental 3-point bending studies. *Purpose***:** To reveal the association between the direction of the force and the fracture pattern, with and without axial loading. *Material and methods*: A Dynatup Model POE 2000 (Instron Co.) low energy pendulum impact machine was utilized to apply impact loading on fresh pig femoral bones (n=50). The bone clamp shaft was adjusted to position the bone for three-point bending with and without additional bone compression. Four different directions of the force were applied: anterior, posterior, lateral, and medial. *Results:* the impacted aspect can be distinguished from the non-impacted aspects based on the fracture pattern alone (the most fractured one); the impact point can be identified on bare bones (the area from which all oblique lines radiate and/or the presence of a chip fragment). None of our experiments (with and without compression) yielded a "true" butterfly fracture, but instead, oblique radiating lines emerged from the point of impact (also known as "false" butterfly). Impacts on the lateral and anterior aspects of the bones produce more and longer fracture lines than impacts on the contralateral side; bones subjected to an impact with axial loading

are significantly more comminuted and fragmented. Under axial loading, the number of fracture lines is independent of the impact direction. Our study presents an experimental model for fracture analysis and shows that the impact direction and the presence of axial loading during impact significantly affect the fracture pattern obtained.

Introduction

Knowledge on long bone failure mechanisms and fracture patterns may assist anthropologists and physicians in legal (forensic) medicine, i.e., in identifying the trauma that caused an injury. Traffic accidents, for example, is of major importance since road traffic injuries are the leading cause of death worldwide among young people aged 10-24 years, with nearly 400,000 people under the age of 25 dying in the world's roads [39]. Analysis of bone fractures may assist in reconstructing the location of pedestrians relative to the vehicle and their position (standing or recumbent), moving phase (standing or moving), the impact direction, the type of collision (front, corner, sideswipe), and the type and speed of the vehicle. Analyses of the lower-extremity bone fractures are of particular relevance in car-to-pedestrian hits, since they reflect the actual location of the pedestrian relative to the vehicle [29].

Many factors may be involved in the type and extent of the fracture observed, e.g., intrinsic and extrinsic, the soft tissues and material type around the bone and the impact surface type and size [5], the height of the fall, and the initial energy [6], as well as the velocity of both the car and the pedestrian (standing, walking, and

running) [24]. Better understanding the combined forces that acted on the bone, i.e., tension, compression, shearing, torsion, and bending is the key for identifying the a priori events that led to the fractures.

Fracture patterns are usually classified into 6 classic types: transverse, oblique or butterfly, spiral, segmental, and comminuted. This classification of fracture patterns is largely derived from the medical literature where determination of the stability of the injury, the probable extent of associated soft tissue damage, and the prognosis for recovery are the primary motivations [10]. However, using this classification of fractures to reconstruct the causes of trauma is not straightforward.

The biomechanics of long bones has been studied since the 19th century. However, with long bones most works have dealt with the quasi-static testing of standardized specimens, in order to determine the material properties rather than the fracture pattern (e.g., [23][33][34][38]). In 1880, Messerer found that the cracking or tearing of the bone generally occurred on the convex (tension) side of the bone. In bones exhibiting a significant bend, crushing was evident on the concave (compression) side, at the point where the load was applied, before a tearing or tension fracture occurred [20] (Cited from Kress et al., 1995 [18]). Evans and Lissner [9] further emphasize, through stresscoat studies, the significance of tensile stresses as the cause for bone failure. One of the most detailed discussions of tibial impact, including impactor weight, size, direction, and velocity was carried out by Nyquist et al. [23]; however, the information regarding the fracture pattern was very general and meager. Another important study on fracture patterns and their relation to impact conditions was carried out by Kress et al. [18]. Since these early studies, numerous other static test results have been published and much of these data can be found in the engineering literature. Many authors have aimed at listing certain patterns of fractures

following mechanisms of loading (e.g., [14][21][36]). Most studies describe and define fracture types in relation to the direction of loading and the loading type applied, e.g., a transverse fracture resulting from a bending load, an oblique fracture resulting from compression, and a butterfly fracture resulting from a combination of bending and compression loads [3][10][11][12][31]. Although there is a consensus regarding the mechanism that produces certain fracture patterns, competing theories exist in the medical literature in relation to others. In addition, most studies analyzing fracture patterns in 3-point bending did not include additional axial compression loading, defined as when the thigh receives a lateral blow when bearing weight, for example, pedestrians injured by vehicles. In addition, the information regarding the nature of the specimens studied was incomplete, and the precise site of impact was not reported.

Currently, there is no a single study that has inclusively examined the morphological and metrical characteristics of fractures with regard to the impact direction of the force applied and the effect of axial loading on the fracture pattern from a forensic perspective, simulating a situation occurring in pedestrian road traffic accidents.

Objectives of the study

The objectives of the study were to reveal the association between the direction of impact loading and the bone fracture pattern and to assess how additional axial loading influences a fracture pattern, by simulating body weight on a leg (as in a standing position) during impact.

Materials and methods

Experimental set-up: The Dynatup Model POE 2000 (Instron Co.) low energy pendulum impact machine, shown in Figure 1, was utilized to apply impact loading on pig femoral bones. Custom-made supports for holding each bone in place during loading were fabricated. The clamp shaft was designed to support the bone while the impact load was oriented perpendicularly to the longitudinal axis of the bone (Figure 2). The bone clamp shaft was adjusted to position the bone for three-point bending with additional bone compression, simulating body weight on a leg (as in a standing position). The compression forces (in relation to the long axis of the bone) were generated by moving the clamp plates located at the edges of the bone; the exact amount of compression forces was adjusted and monitored using the Tension Compression Load Cell (Vishay Tedea-Huntleigh 615) and a digital monitor (Rinstrum 310). Two adjustable supports allow the inner loading span along the bone shaft to be altered, depending on the bone size (Figure 2). Preparation of bones**:** Fresh femora of young pigs (5-6 months old) were exposed to the impact loading. Juvenile bones were selected for this study since road traffic injuries are the leading cause of death worldwide among young people aged 10-24 (World Health Organization) [39]. The pig bones were obtained fresh and almost clean from an abattoir (on the day of slaughter). The specimen preparation included careful separation of remnant muscles and all other soft tissues from the bones, including the periosteum. All bones were visually examined for macroscopic defects, skeletal disease, or pre-fractures, and later were stored frozen at −20 °C until testing. The bones were labeled and their lengths and mid-shaft dimensions were measured. In order to hold the bones stable in the compression clamps so that compression forces could be applied on all articular areas, the bones' epiphyses were embedded in transparent polyester resin (Erco E-

16®). Preceding the coating process, the bones were thawed with water to room temperature and stored in a water tank during processing. Four drops of accelerator solution and 3 ml of hardener solution were inserted into a small plastic container containing 120 ml of liquid transparent polyester in order to prepare the polyester solution (the plastic containers were covered on the inside with a thin layer of Vaseline in order to prevent the polyester from sticking). The bones were inserted into the empty plastic container with their longitudinal axis perpendicular to the base of the container and were handled in a fume hood, using a stable handle. In order to cover the distal epiphysis with polyester, both condyles, in all tests, were set to meet the bottom of the plastic container (leveling process); the plastic containers were leveled horizontally using a simple level bar. Following the leveling process, the polyester solution was poured into the plastic container and left for 30 minutes until drying and cooling were complete. Testing procedure: A custom-made impactor-body (tup) was connected to the pendulum of the impact machine. All bones were fractured in three-point bending under wet conditions. The inner loading span was adjusted consistently to be 8 cm. The compression force applied along the long bone axis through the clamps was adjusted consistently to be 25 kg (assuming equal compression forces on each leg). The bones were set in the compression clamp with their longitudinal axis perpendicular to the pendulum movement. The tup of the pendulum (impact body), a half-cylinder shaped-body (10 mm diameter) composed of stainless steel was adjusted to meet the bone in its mid-span point (the center of the bone). The longitudinal axis of the tup was oriented perpendicular to the longitudinal axis of the bone, creating a contact-point impact. The energy of the pendulum (in Joules) was calculated based on its potential energy at the initial height where the pendulum was elevated:

(1) $$E_P = mgh$$

M is the mass (kgm), *g* (9.81 m/sec^2) is the gravity acceleration, and *h* (m) is the height from which the pendulum was released.

The mass (*m*) and the pendulum height (*h*) in Eq. 1 were calculated by

(2) $$W = mg$$
$$h = L(1 - \sin(90 - \theta))$$

W is the weight of the body-mass, *L* is the length of the pendulum arm, and θ is the angle of the body-mass elevation.

The velocity at the impact was calculated by assuming that all the potential energy was transferred into kinetic energy (Table 1). That is:

(3) $$mgh = \frac{1}{2}mv^2$$

The tests: In order to reveal the association between impact directions and fracture patterns, 40 bones were fractured from four different directions. All tests were conducted without additional axial loading. In order to reveal the effect of axial loading on the fracture pattern, 10 bones were laterally impacted under axial loading (compression). All five tests were conducted under a 3.47 m/sec velocity impact (10 bones in each group).

The following five tests were applied:

Test-1: Lateral impact.

Test-2: Anterior impact.

Test-3: Medial impact.

Test-4: Posterior impact.

Test-5: Lateral impact under axial loading (compression).

The following independent variables were measured either prior or following testing:

1. **Bone maximum length**: Prior to testing, the maximum length between the head of the femur and the condyles was measured.
2. **Cross-sectional dimensions** at the impact point: The lateral-medial and anterior-posterior diameters were measured prior to testing as well as the cortical bone thickness following testing. Since the lateral-medial diameters were significantly higher (4%; $p<0.001$) than the anterior-posterior diameters, the moment of inertia of a tube was determined when bending was considered, based on the direction of impact. In the case of impact from lateral to medial, the thicknesses of the lateral cortex (T1) and the medial cortex (T2) were used. In the case of impact from anterior to posterior, the thickness of the anterior cortex (T4) and the posterior cortex (T3) were used

(4) $$I = \frac{\pi(d_E^4 - d_I^4)}{64}$$

= External lateral-medial diameter,

Internal lateral-medial diameter,

$d_I = d_E - (t_i + t_j)$

Thickness of the lateral cortex (T1) + the thickness of the medial cortex (T2)

Thickness of the posterior cortex (T3) + the thickness of the anterior cortex (T4)

The following dependent variables were measured following testing:

1. The number of fracture lines: Any fracture line longer than 1 cm was recorded. Fracture lines may appear in different forms: longitudinal, oblique, transverse, or polygonal (see below for more details). Fracture lines were defined as follows:

d_E

$d_I =$

a. Longitudinal lines: Straight lines running proximally or distally, parallel to the bone longitudinal axis, toward the epiphysis. The longitudinal lines may appear in all aspects of the bone (medial, lateral, anterior, and

$t_i =$ posterior), but usually they can be found in the area of impact (C-longitudinal line), in the contralateral aspect (CL- longitudinal line), or in both

$t_j =$ aspects. Related observations and measurements include the presence, number, and location (Figure 3).

b. **Oblique lines:** Fracture lines running at an angle to the long axis of the bone. Oblique lines usually run proximally or distally toward the epiphysis and to other aspects of the bone. Oblique fracture lines were defined according to their direction and propagation, for example, proximal oblique medial (POM) refers to an oblique line (O) running towards the proximal epiphysis (P) from the impact point to the medial aspect (M) of the bone. The area between two oblique lines is "the **polygon"**; their numbers, location, and length (mm) have also been recorded (Figure 3).

c. Transverse lines: A horizontal line fully encircles the diaphysis. It appears ether straight or fractured. It is recorded either as present or absent (Figure 3).

2. Chip fragment: A missing bony part at the point of impact. Related observations and measurements include the presence and size (circumferential length (mm)) (Figure 3).

Bone preparation for analysis of fracture lines: the post-test procedure: The cleaning process consisted of five hours of boiling in water with detergent, 20 minutes soaking in 35% Hydrogen Peroxide, and 10 minutes rinsing with water (before the cleaning process, the polyester coating was removed). All bone fragments were placed on blotting paper and allowed to dry for 24 hours. Following the cleaning and drying processes, all bony fragments were reassembled to form a complete bone using UHU adhesive.

Analysis of fracture lines: The fracture lines were quantitatively analyzed by measuring the fracture lines' length using Microscribe® G2X 3D digitizers directly on the reassembled bones. The X, Y, and Z coordinates of the deviation points along

each segment of the fracture line were obtained. The length between each pair of points was calculated by the 3D Pythagoras Theorem. The total fracture line length was the sum of the segments' lengths.

Statistics: The statistical analysis was carried out using SPSS V15. Descriptive statistics were applied on all data. The ANOVA test was used to analyze the differences between the group means. A Student's t-test was carried out to detect significant differences in the parameters' means between two groups. The Chi-square test was carried out to reveal associations between categorical variables. The Kruskal-Wallis test was used to evaluate between-group differences in non-parametric variables. The P value was set at $p<0.05$.

Results

This study describes and analyzes fracture patterns in two modes: qualitative and quantitative. In the quantitative mode, the fracture line measurements are summarized. In the qualitative mode, schematic illustrations of the fracture patterns are presented for each test. All four aspects of the bone: anterior, posterior, lateral, and medial are presented and discussed.

The association between the fracture pattern and the impact direction

The data on the relationships between the fracture characteristics and different impact directions appear in Tables 1-4. Bone and fracture line metrical characteristics in different impact directions are presented in Table 1. No significant differences in the cross-sectional moment of inertia between the femora in the four tests carried out were found. This implies that factors other than morphometrical differences in the femur characteristics are responsible for the results in the different tests. The number

and length of the fracture lines are clearly associated with the impact direction: the lateral impact produces the highest number of fracture lines and the longest ones, whereas the posterior impact produces the smallest number of fracture lines and the shortest ones (Table 1). The length and number of fracture lines were similar in bones impacted from the medial and anterior sides (Table 1). A chip fragment on the point of impact was found in bones subjected to medial, lateral, and anterior impacts. The largest chip fragment was found on the anterior aspect. Chip size and the number of fracture lines were independent of the impacted aspect: lateral, medial, anterior, and posterior (Table 1). Significant associations were found between the direction of impact and the number of longitudinal lines and the presence of chip fragments (Table 2). The largest number of longitudinal fracture lines (n=9) was found in bones impacted from the lateral side (Table 2). Most longitudinal lines, however, were found on the contra lateral side (medial side) (Table 3). Similar numbers of longitudinal lines (n=7) were found in bones subjected to medial and anterior impacts (Table 2). In these groups, the longitudinal lines were found mostly on the impact side (57.5% and 72%, respectively) (Table 3). The smallest number of longitudinal lines was found in bones impacted on the posterior aspect (n=3) (Table 2). The largest numbers of polygons were found in bones impacted on their lateral side, followed by bones subjected to an anterior aspect and finally, bones subjected to posterior and medial impacts (Table 2). Chip fragments were present in 70% of the bones subjected to an anterior impact, in 50% of bones subjected to a lateral impact, and in 30% of bones subjected to a medial impact. No chip fragments were found in bones subjected to a posterior impact. Distributions of longitudinal line locations by impact direction appear in Table 3. The average numbers of fracture lines by bone aspect and impact direction appear in Table 4. There is a clear relationship between the direction of the

impact and the number of fracture lines regarding the different aspects of the bone. Except in the case of posterior impacts, most fracture lines are located on the impacted aspect.

A schematic illustration of the most common fracture pattern, following a lateral, anterior, medial, and posterior impact (tests 1-4), is presented in Figures 4-7. In general, only bones subjected to lateral (Figure 4) and anterior (Figure 5) impacts present a multifragment "false" butterfly pattern, as compared with the relatively fragmental transverse/oblique pattern in bones subjected to a medial (Figure 6) and posterior (Figure 7) impact. In bones subjected to a lateral and anterior impact the transverse T line is absent. Bones subjected to a lateral impact are fractured the most and present a significantly greater number of long fracture lines, including "false" butterfly fragment (four oblique-spiral lines), a large number of longitudinal lines in almost all aspects, and a moderate sized chip fragment at the point of impact (Figure 4). As compared with bones subjected to a lateral impact, bones subjected to anterior impact also present a multifragment "false" butterfly pattern, however, with a smaller number and shorter fracture lines (Figure 5). The most marked difference between bones subjected to an anterior and lateral impact is related to the chip fragment. In both cases, the chip fragment is located on the impact aspect; however, it is much larger and more common in bones subjected to an anterior impact (Figure 4 vs. Figure 5). Only in bones subjected to an anterior impact is there a clear resemblance between the chip fragment shape and the impact body morphology. Bones subjected to a medial and posterior impact present a fragmental transverse/oblique pattern (Figures 6, 7); however, in bones subjected to a medial impact (Figure 6), a complete circumferential transverse line is present and a butterfly pattern is less common. In both cases, only inferior oblique lines are present; however, in bones subjected to a

medial impact, the oblique lines originate from a moderate sized chip fragment rather than ones from a distant origin (such as a short transverse line) as in bones subjected to a posterior impact. The chip fragment in bones subjected to a medial impact is of moderate size as in bones subjected to a lateral impact; however, in bones subjected to a medial impact a long longitudinal line is usually present at the point of impact, running superiorly or inferiorly toward the epiphysis. Bones subjected to a posterior impact present the least number of fracture lines, usually with a short transverse line on the impact aspect only (Figure 7). In all bones subjected to a posterior impact, the chip fragment at the point of impact is absent, and as in bones subjected to a medial impact, only inferior oblique lines are usually present, explaining why the butterfly pattern is less common (Figure 7).

The association between the fracture pattern and the presence of axial loading

Mean values (±SD) for bones and fracture characteristics relating to the association between the fracture pattern and the presence of axial loading appear in Table 5. Lateral impact with additional axial loading (compression) produced significantly more fracture lines than did lateral impact without additional axial loading. Bones subjected to an impact without axial loading manifest on average one longitudinal line on the contra lateral aspect. This line is absent in bones subjected to an impact with axial loading. The bone-chip fragment at the point of impact is significantly larger in bones tested under axial loading. Differences, although not significant, were also found in relation to the fracture line length (Table 5). The average number of fracture lines by bone aspect and axial loading in bones impacted from the lateral impact appear in Table 6. Under axial loading, the number of fracture lines is similar on all aspects of the bone; however, without axial loading the number of fracture lines on the impacted side is significantly greater than on the other aspects (Table 6).

A schematic illustration of the most common fracture pattern following lateral impact with axial loading is shown in Figure 10. As compared with a comminuted or multifragment "false" butterfly fracture in bones subjected to a lateral impact with axial loading, fractures in bones subject to a lateral impact without axial loading, although also presenting a butterfly pattern, are significantly less comminuted and fragmented (Figure 4). With a lateral impact without axial loading, the butterfly fragments appear smaller (the oblique lines exhibit a low degree of propagation not reaching the metaphysis area near the epiphyses). On the lateral (impacted) aspect of bones subjected to an impact without axial loading, the chip fragment is smaller and the fracture line between the distal oblique-radial lines and the transverse line is absent. In these bones, a short longitudinal line is present at the point of impact, running proximally from a small chip fragment. In cases of impact without axial loading, only a single longitudinal line is present between the oblique-radial lines on the anterior aspect as compared with the presence of numerous radiating lines in bones following an impact with axial loading (see Figure 10).

Discussion

In all tests conducted in this study, the impacted aspect (lateral, medial, anterior, or posterior) manifested a different fracture pattern from that seen in the non-impacted aspects. This phenomenon can be used to identify the impact direction, i.e., the impact point is the area from which all oblique lines radiate. Sometimes it can also be identified by the presence of a chip fragment. In all experiments carried out, except for bones subjected to a posterior impact, the impacted aspect was also the most fractured one.

In this section, three major findings will be discussed: a. the presence of "V-shaped" radiating fracture lines, b. the differences in the fracture pattern among the impacted

aspect (anterior, lateral, medial, and posterior), and c. the effect of axial loading on the fracture pattern.

V-shaped fracture lines: None of our experiments (with and without compression) yielded a "true" butterfly fracture, i.e., apex (origin) of V-shaped lines is located contralateral to the impacted surface. Butterfly fractures are commonly seen in the lower extremities when the thigh or calf receives a lateral blow when bearing weight, as with pedestrians injured by vehicles [11]. Assuming that the bone is weaker in tension than in compression, one would expect to find a transverse fracture line originating on the contralateral side of the impact and a "true" butterfly pattern following bending. In this study, however, no "true" butterfly pattern was identified but rather a "false" butterfly pattern (a wedge-shaped fragment where the apex and not the base is directed toward the impact site). This "false" butterfly fracture pattern was manifested in our study by two oblique lines running from the point of impact superiorly and inferiorly toward the contralateral side: DOA and POA or DOP and POP with a lateral impact (Figure 4) and POM and DOM or POL and DOL with an anterior impact (Figure 5). A V-shaped radiating fracture pattern (as described above) is seen when failure first occurs at the impact site [2]. This is consistent with studies on vehicle-pedestrian accidents, showing that a “false” wedge-shaped fracture is more common in cases where the area of contact between the limb and the vehicle elements is very small [25] (cited from Teresinski, 1999 [37]). Butterfly fractures are commonly used in forensic cases for establishing the position of a pedestrian in relation to a motor vehicle [37]. The mechanism underlying this fracture was the subject of Messerer’s study in the late 19th century [20]. Thereafter, this rule concerning the location of the base of the wedge (from the impact side) and its apex (according to the force direction) became the most common and almost dogmatically

a ‘standard’ in forensic medicine for reconstructing the direction of the impact [7][8][15][37][35]. Nevertheless, as has also been found in our study, there is growing evidence suggesting the presence of a reversed phenomenon, i.e., the apex, and not the base, is sometimes directed toward the impact site (commonly called a “false" butterfly fracture, although we prefer to refer to this fracture "radiating lines"). For example, Spitz and Russell (1980), in their study on pedestrian leg impact [36], found that sometimes even a “false” wedge-shaped fragment can be seen. This observation was repeated in other studies [16][18][27][28]. Rich (2005) claimed that a typical bending fracture (Messerer`s wedge) can indicate the direction of impact only when the bone was bent at the moment of impact [29]. Interestingly, in 1963 Patscheider proved experimentally the possibility of the occurrence of “false” indirect wedge-shaped tibial and femoral fractures by hitting rigidly fixed human and animal bones with a weighted pendulum [25]. In 1999 Teresinski and Mydro examined 14 femurs with wedge-shaped fractures, following pedestrians' car accidents, to evaluate the evidential value of wedge-shaped fractures: in only 50% of the cases were "true" wedge fractures (“Messerer’s fractures”) found; 21% of the cases manifested "false" wedge fractures and the rest had the wedge fracture at the impact side [37]. It is noteworthy that the lack of a true butterfly fracture in our study could be partially due to two factors: the absence of protective soft tissue around the tested bone, and the lack of compression forces. With regard to the former, first, it should be remembered that "false" butterfly fractures have been reported in pedestrian car accidents as well [37], second, "true" butterfly fractures were not produced even when the impact body was covered with soft material (mimicking the periosteum and muscles around the bone). Regarding the latter, our experiments with compression forces did not produce "true" butterfly fractures. In this regard, it is worth mentioning Rich et al.’s (2005)

study in which they claimed that they routinely produced oblique, transverse, and butterfly fractures following simple 3-point loading of bare long bones with absolutely no axial or torsional loading. All these observations imply that more experimental research on the etiology of butterfly fractures is required before they can be used as credible evidence in forensic cases.

The fracture pattern and the impacted aspect: In the current study we found considerable differences in the fracture pattern and intensity between opposite bone aspects (Table 4). When the lateral aspect is impacted, the mean fracture line is 4.3, whereas when the medial aspect is impacted, the mean fracture line is 2.9. This phenomenon is also observed on the anterior-posterior dimension of the bone, with a mean fracture line of 4.2 on the anterior aspect and 2.0 on the posterior. The reasons for the above-mentioned variability in the fracture pattern and intensity among impacted areas are related to two factors: the size and shape of the impact body and the shape of the bone (on both the transverse and longitudinal planes). Since the impact body is rectilinear, 12 long (Figure 8) and the shaft is not a true cylinder (i.e., on the transverse plane it manifests a relatively flat posterior aspect and an arched anterior aspect, whereas on the longitudinal plane it arches laterally), the produced fracture pattern following an impact will greatly depend on the extent of the contact area between these two bodies. The round anterior aspect produces a small contact area between the bone and the impact body (Figure 9). In an anterior impact, the relatively small contact area acts to increase the impact stress (concentrated in a small area), which eventually produces more fracture lines, broad propagation, and a large chip fragment. This also explains why the chip fragment is greater on the anterior impact. The flat posterior aspect produces a large contact area between the bone and the impact body (Figure 9). In the posterior impact, with the same force applied, the

large area of the bone that comes in contact with the impact body dissipates the energy; hence, fewer fracture lines with decreased propagation, and with no chip fragments are produced. The same scenario can be applied to the difference in the fracture pattern and intensity between the lateral and the medial aspects; this time however, the differences in shape are mainly with regard to the longitudinal plane, the lateral aspect being arched, whereas the medial side is rather flat (Figure 9). This study clearly shows that in analyzing the association between the impact and the fracture pattern, the shape, velocity, and mass of the impact body are only part of the story; the general shape and size of the bone, its adjacent structures (periosteum, muscles' mass), and the direction of the impact must also be taken into consideration.

The association between the fracture pattern and the presence of axial loading: In the current study we have shown that bones subjected to an impact with axial loading are significantly more comminuted and fragmented, the butterfly fragments are larger, and the number of fracture lines is similar in all bone aspects, compared with bones impacted without axial loading. In compression or axial loading, two forces act towards each other along the same line [22]. These forces cause high shear stresses along oblique planes that are oriented at about 45 degrees from the long axis [4]. An oblique fracture usually results from the combination of angulation and axial compressive forces of moderate intensity [10] or a combination of torsion and bending (when bending is the dominant loading factor) [30]. Since bones under axial loading experience shear stresses, the primary energy stored prior to impact is greater. This may explain the significantly more comminuted fracture pattern in bones subjected to an impact with axial loading, i.e., resulting from the need to dissipate a larger amount of energy through fracture (energy stored from the compression forces and the potential energy from the impact). Noteworthy is that a "false" butterfly (or

V-shaped radiating fracture pattern) was also obtained in cases of impact with axial loading. Moreover, the transverse line fracture (not present under 3-point bending without compression) appears on the impacted side and not on the contralateral side (as expected in a true butterfly fracture). This is in concordance with other studies that have shown that a transverse fracture type can result from a force producing bending [27] or severe angulations, but not necessarily under compression from the normal weight-bearing functions [10]. This discrepancy (between "true" vs. a "false" butterfly fracture) implies that once a fracture analysis is considered for forensic purposes, the forensic team should consider various factors, e.g., the shape of the bone (some people have more concave bones than others), the thickness of the muscles' tissue, mass, and orientation, the weight of the individual (the extent of the compression load), age, and sex, among other factors.

Experiments including three-point bending with axial (compression) loading is important because they simulate an impact to the lower limb long bone when walking or running (in the "swing phase"), contrary to falling from a chair, or in cases of impact to the arm in a resting position, i.e., standing, sitting, or lying down.

Justification for using pig bones

The similarities between pig and human bones, mainly with regard to their shape, microstructure (i.e., Haversian system) [13], and density [1] make pig bones an excellent model for assessing human bone mass and strength [26]. Immature pigs at their early stage of development manifest a plexiform bone structure (a type of primary bone tissue). Nevertheless, by the age of 5-6 months, most of the cortical bone area is of the Haversian type, as in humans.

Summary: This study, to the best of our knowledge, is the first to examine experimentally the association between the direction of force and the effect of axial

loading on bone fracture patterns, from a forensic perspective. Our study can serve as a basic model for fracture analysis, as well as a core principle for future studies and forensic case analysis. Nevertheless, when our results are used for interpreting the impact in forensic cases, the forensic staff should be aware of their limitations (see the limitation section). In a forensic context, the ability to identify the impact direction is of major importance in both pedestrian traffic accidents and violent assaults. The reconstruction can reveal the position and the location of the victim relative to the vehicle in cases of pedestrian traffic accidents, or the assailant in cases of violent assaults. The ability to distinguish between fracture patterns whether or not the impacted bone is under axial loading (compression) is important in evaluating both pedestrian traffic accidents and violent assaults. Correct forensic reconstruction can reveal the position of the victims (standing or recumbent) and their moving phase (standing or moving) and can determine whether they fell on or were hit by an object.

Limitations of the study

This study is sample specific and further validation (by an independent laboratory using other samples) is required in order to develop an appropriate prediction model for bones in general, and human bones, in particular. For the sake of simplicity, bones were impacted at mid-shaft. Other sites of impact may yield different results. It should be recall that the setting of the experiment itself may affects the results, i.e., the direction of impact simulated by the Instron apparatus was applied perpendicular to the bone diaphysis; hence, different impact orientations might result in different fracture patterns. In addition, as we have previously shown, a blow applied to a bone shaft surrounded by soft tissue may not produce the same fracture pattern as when a blow is applied to a clean bone shaft, although the pattern of the fracture will retain its general characteristics [5].

References

[1] Aerssens, J., Boonen, S., Lowet, G., Dequeker, J. (1998). Interspecies differences in bone composition, density, and quality: Potential implications for in vivo bone research. *Endocrinology* 139:663-70.

[2] Dirkmaat, D. (2012). Interpreting Traumatic Injury to Bone in Medicolegal Investigations. In: A Companion to Forensic Anthropology. 1st ed. London, Blackwell Publishing Ltd.

[3] Brumback, R. J. (1996). The rationales of interlocking nailing of the femur, tibia, and humerus. *Clinical Orthopaedics and Related Research* 324:292-230.

[4] Browner, B. D. (2009). *Skeletal Trauma.* 4th ed. Philadelphia, W. B. Saunders Company.

[5] Cohen, H., Kugel, C., May, H., Medlej, B., Stein, D., Slon, V., Brosh, T., Hershkovitz, I. (2017). The effect of impact tool geometry and soft material

covering on bone fracture pattern in children (accepted for publication in *International Journal of Legal Medicine Journal*).

[6] Cohen, H., Kugel C., Slon, V., May, H., Medlej, B., Stein, D., Hershkovitz, I., Brosh, T. The impact velocity and bone fracture pattern: forensic perspective (2016). *Forensic Science International* 266:54–62.

[7] Dürwald, W. (1966). Gerichtsmedizinische Untersuchungen bei Verkehrsunfällen. Thieme: VEB Georg Leipzig.

[8] Eubanks, J. J., Hill, P. F. (1999). Pedestrian accident reconstruction and litigation, Lawyers & Judges Publishing Co.

[9] Evans, F. G., Lissner, H. R. (1948). Stresscoat deformation studies of the femur under vertical static loading. *The Anatomical Record* 101:225-241.

[10] Galloway, A. (1999). *Broken bones: Anthropological analysis of blunt force trauma.* Charles, C. Thomas Pub, Ltd.

[11] Gozna, E. R. (1982). *Biomechanics of musculoskeletal injury*. Baltimore, Williams & Wilkins.

[12] Harkess, J. W. (1975). Principles of fractures and dislocations. In: *Fractures.* Edited by C. A. Rockwood and D. P. Green. Philadelphia, J. B. Lippincott.

[13] Hillier, M. E., Bell, L. S. (2007). Differentiating human bone from animal bone: a review of histological methods. *Journal of Forensic Science* 52:249-263.

[14] Johner, R., Wruhs, O. (1983). Classification of tibial shaft fractures and correlation with results after rigid internal fixation. *Clinical Orthopedics* 178:7-25.

[15] Karger, B., Teige, K., Fuchs, M., Brinkmann, B. (2001). Was the pedestrian hit in an erect position before being run over? *Forensic Sci Int* 119:217–220.

[16] Kozlov, S. N., and Yurasow, A. G. (1981). Neprjamye perelomy bedra pri udare bamperom avtomobilja. Sudebno-Medicinskaja Ekspertiza t. XXIV, s. 13-15.

[17] Kieser, D.C., Riddell, R., Kieser, J.A., Theis, J.C., Swain, M.V. (2014). Bone micro-fracture observations from direct impact of slow velocity projectiles. *J Arch Milit Med* 2(1): e15614.

[18] Kress, T. A., Porta, D. J., Snider, J. N., Fuller, P. M., Paihogios, J. P., Heck, W. L., Frick, S. J., Wasserman, J. F. (1995). Fracture patterns of human cadaver long bones. *International Research Counsel on the Biomechanics of Impact.* pp. 155-169.

[19] Levine, R.S. (1986). An introduction to lower limb injuries in biomechanics and medical aspects of lower limb injuries. SAE technical paper #861922. Society of Automotive Engineers, Inc., pp. 23-29.

[20] Messerer, O. (1880). Uber Elasticitat und Festigkeit der mensch lichen Knochen. Stuttgart, Cotta, pp. 1-100.

[21] Rockwood, C.A., Green, P. D., Wilkins, K. E., Robert, W., Heckman, B. G. D., Court-Brown, C. M., Beaty, J. H., Kasser, J. R. (2001). Rockwood And Green's Fractures in Adults (2 volume set). 5th ed. Lippincott Williams & Wilkins Publishers.

[22] Nordin, M., Frankel, V. H. (2001). *Basic biomechanics of the musculoskeletal system*. Lippincott Williams & Wilkins. 3rd ed., pp. 27-55.

[23] Nyquist, G. (1986). Injury tolerance characteristics of the adult human lower extremities under static and dynamic loading. In: *Biomechanics and*

medical aspects of lower limb injuries. Warrendable, PA: Society of Automotive Engineers, Inc., pp: 79-90. SAE Technical Paper 861925.

[24] Panjabi, M. M., White, III. A. A. (2001). *Biomechanics in the musculoskeletal system*. Philadelphia: Churchill Livingstone.

[25] Patscheider, H. (1963). Über Anprallverletzungen der unteren Gliedmaßen bei Straßenverkehrsunfällen. Deutsche Zeitschrift für gerichtliche Medizin Bd 54, S. 336–366 .

[26] Pond, W., Houpt, K. (1978). The biology of the pig. 1st ed. Ithaca (NY), Comstock Publishing Associates.

[27] Pierce, M. C., Bertocci, G. E., Vogeley, E., Moreland, M. S. (2004). Evaluating long bone fractures in children: a biomechanical approach with illustrative cases. *Child Abuse & Neglect* 28:505-524.

[28] Reilly, T. R., Burstein, A. H. (1974). The mechanical properties of cortical bone. *Journal of Bone and Joint Surgery* 56:1001-1022.

[29] Rich, J., Dean, D. E., Powers, R. H. (2005). *Forensic medicine of the lower extremity.* Totowa, NJ, The Humana Press, Inc.

[30] Rockwood, C. A., Green, D. P., Bucholz, R. W. (2010). Fracture in adults. 7th ed. Lippincott Williams & Wilkins.

[31] Rogers, L. F. (1992). *Radiology of skeletal trauma.* Vol. 1. 2nd ed. New York: Churchill Livingstone, Inc.

[32] Ryan, J. R., Hensel, R. T., Salciccioli, G. G., Pedersen, H. E. (1981). Factures of the femur secondary to low-velocity gunshot wounds. *Journal of Trauma* 21(2):160-162 .

[33] SAE J885 APR86. (1986). Human tolerance to impact conditions as related to motor vehicle design. Society for Automotive Engineers Information Report.

[34] Salerno, A., Trent, R., Jackson, P. L., Cook, M. G. (1995). A rapid and safe method to fix India ink on specimen resection margins. *Journal of Clinical Pathology* 48:689-690.

[35] Spitz, W. U., Fisher, R. S. (1993). Medicolegal investigation of death. 3rd ed. Springfield, Charles C. Thomas .

[36] Spitz, W. U., Russell, S. F. (1980). The road traffic victim. In: *Medicolegal investigation of death: Guidelines for the application of pathology to crime investigation*. 2nd ed. Thomas Books Illinois, pp. 377-405.

[37] Teresinski, G., Mydro, R. (1999). The evidential value of wedge-shaped tibial and femoral fractures in cases of car-to-pedestrian collisions. *Problems of Forensic Sciences* 40(XL):72-85 .

[38] Vincent, E., Tang, C., McKay, H., Oxland, T., Guy, P., Wangm, R. (2007). Strain redistribution and cracking behavior on human bone during bending. *Bone* 40: 1265-1275.

[39] World Health Organization internet site: http://www.who.int/features/factfiles/youth_roadsafety/en/index.html

Fig. 1: Instron POE 2000 pendulum machine used in the current study.

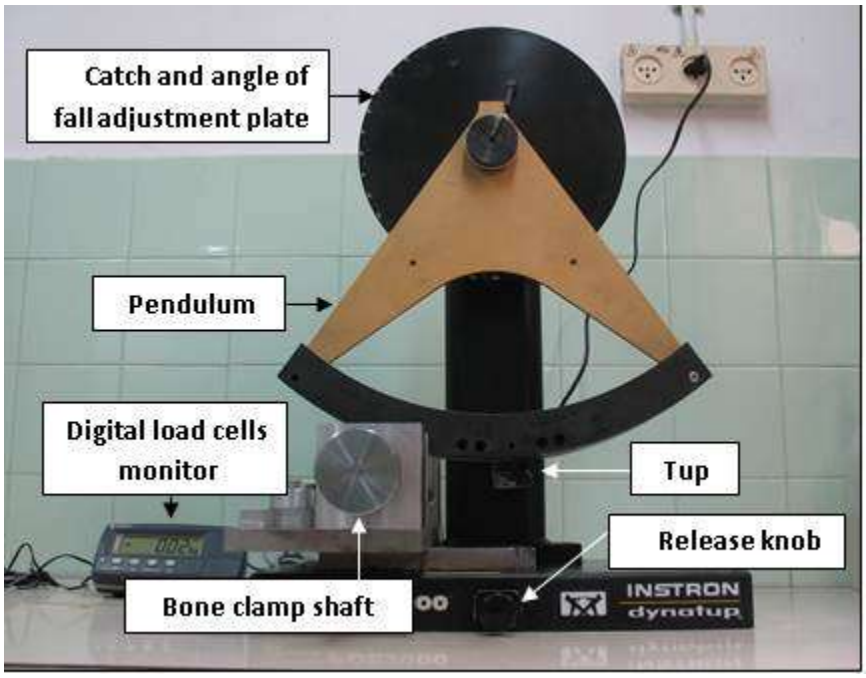

Fig. 2: Bone clamp device. Note that the bone epiphyses are embedded in solid polyester.

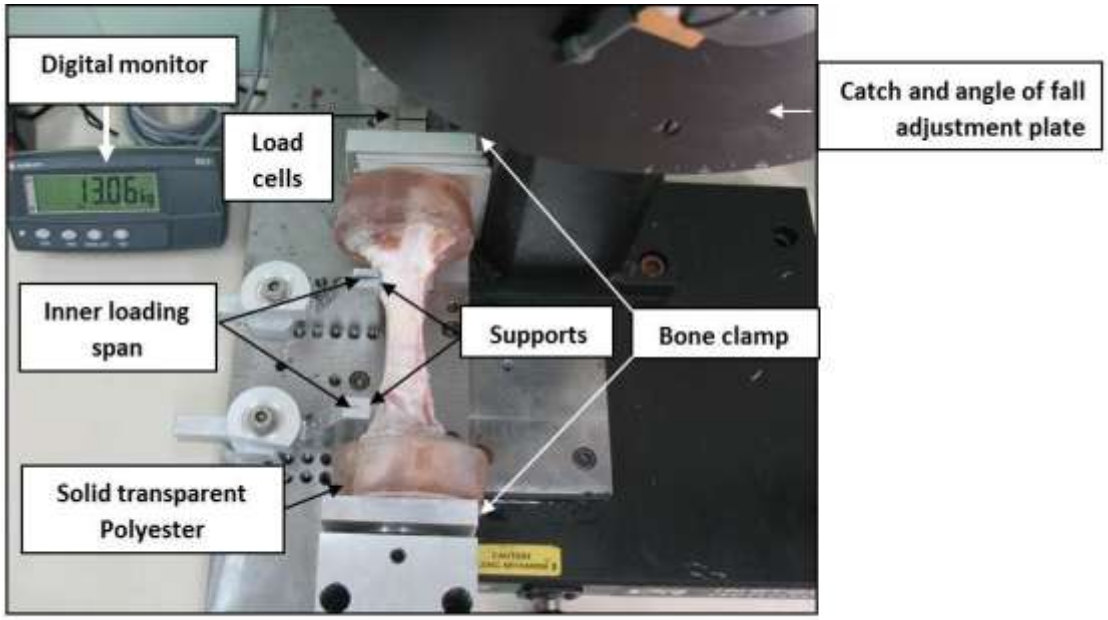

Fig. 3: Major characteristics of the fracture pattern: longitudinal (a); oblique line (b), and transverse line (c); polygon shape (d); missing fragment (chip fragment) at the point of impact (e).

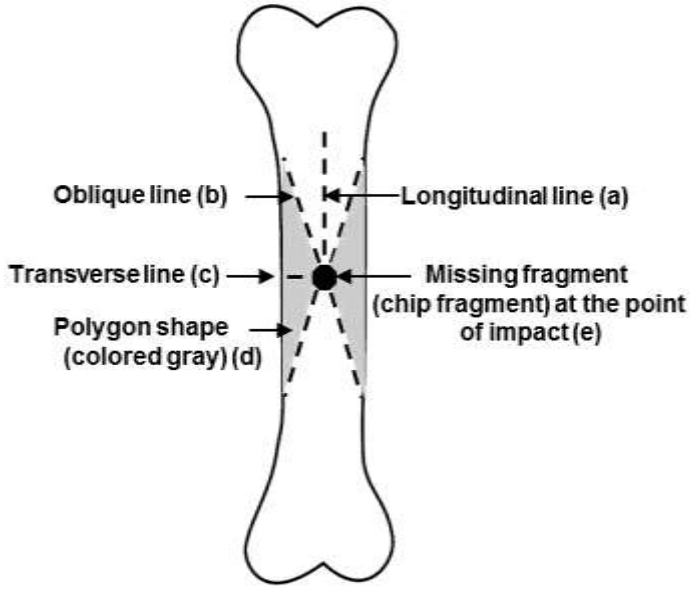

[- - - - -]

[-------]

Fig. 4: Schematic illustration of the fracture pattern following a lateral impact without axial (compression) loading. The primary long oblique lines (long dashed lines =) represent the four long oblique lines emerging from the impact point (**POA =** proximal oblique anterior, **POP** = proximal oblique posterior) (**DOA =** distal oblique anterior, **DOP** = distal oblique posterior). Note the damage to the bone at the impact point, the presence of a short C- and additional longitudinal lines (short dashed lines=). The oblique lines run posteriorly and anteriorly, eventually forming two polygons.

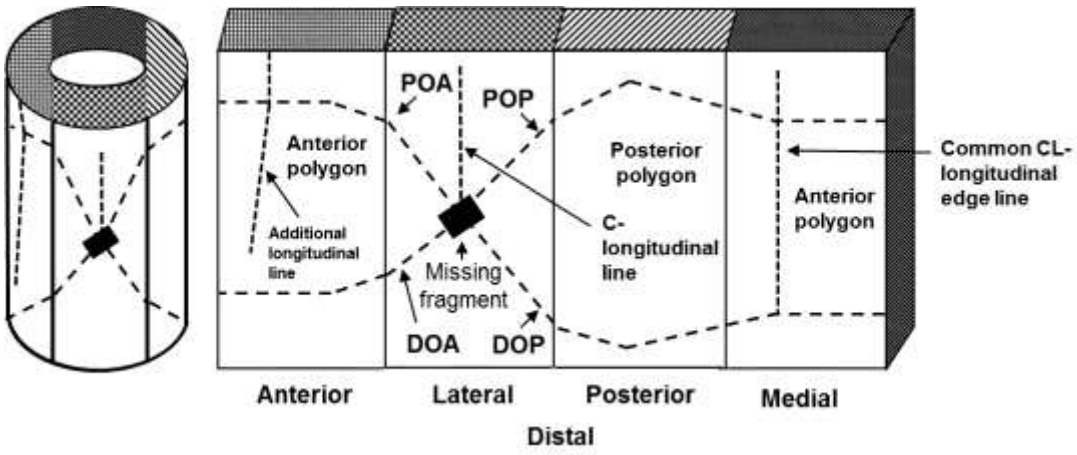

Fig. 5: Schematic illustration of the fracture pattern following anterior impact. Note the large chip fragment at the center and the oblique lines branching out from its margin. The primary long oblique lines (long dashed lines =) represent the four long oblique lines (**POM =** proximal oblique medial, **POL** = proximal oblique lateral) (**DOM =** distal oblique medial, **DOL** = distal oblique lateral). Note the presence of short C- and CL- longitudinal lines (short dashed lines=). The oblique lines run medially and latterly, eventually forming two polygons.

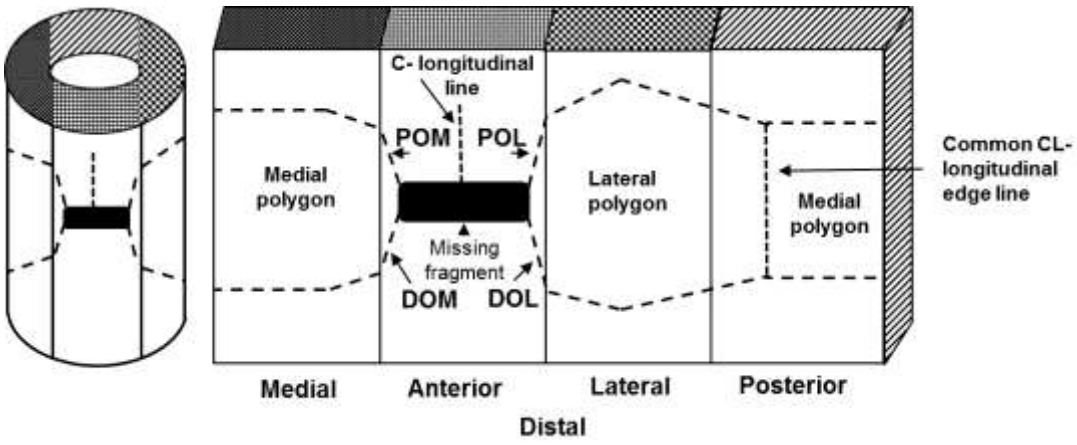

Fig. 6: Schematic illustration of the fracture pattern [- - - -] following medial impact. Note the presence of a complete transverse line, two longitudinal lines emerging from the impact point (short dashed lines=), and the two oblique lines also emerging from this point (**DOA =** distal oblique anterior, [-------] **DOP** = distal oblique posterior) (long dashed lines =).

[-------]

[- - - -]

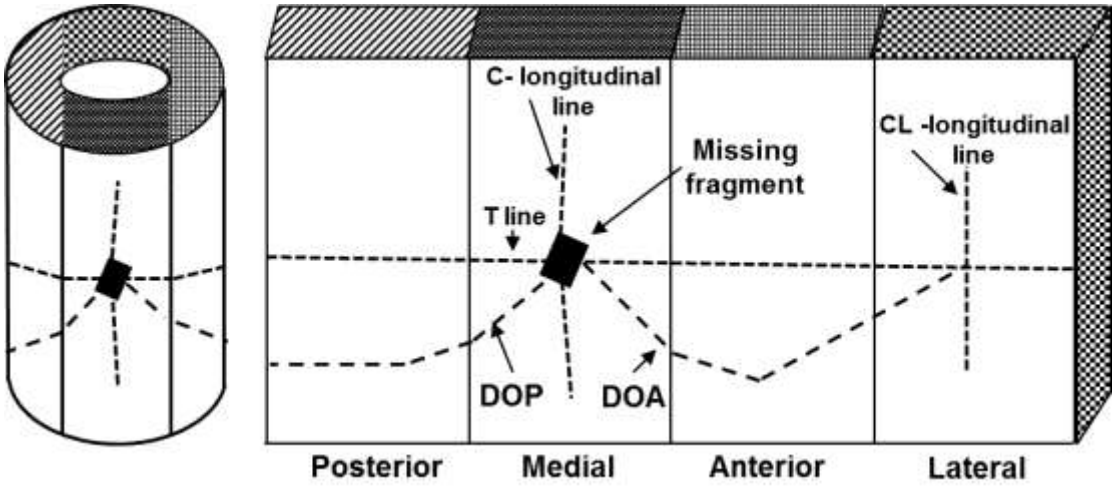

Fig. 7: Schematic illustration of the fracture pattern following posterior impact. Note the short incomplete T line on the impact aspect, C- and CL- longitudinal lines (short dashed lines=), and the two oblique lines starting at both edges of the T line and running obliquely downwards (**DOM =** distal oblique medial, **DOL** = distal oblique lateral) (long dashed lines =).

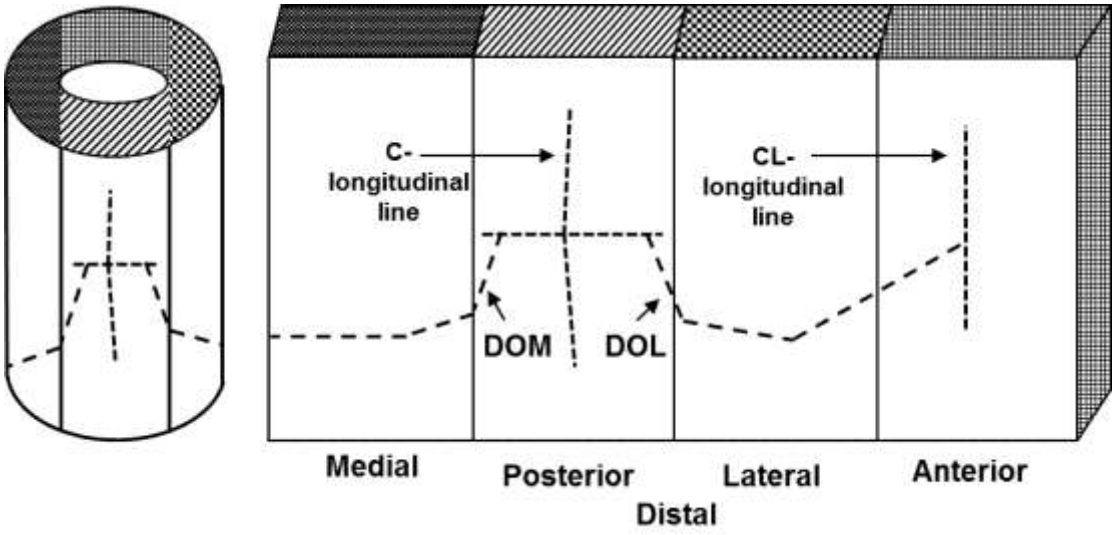

Fig. 8: Schematic illustrations of the impact body.

[-------]

[- - - -]

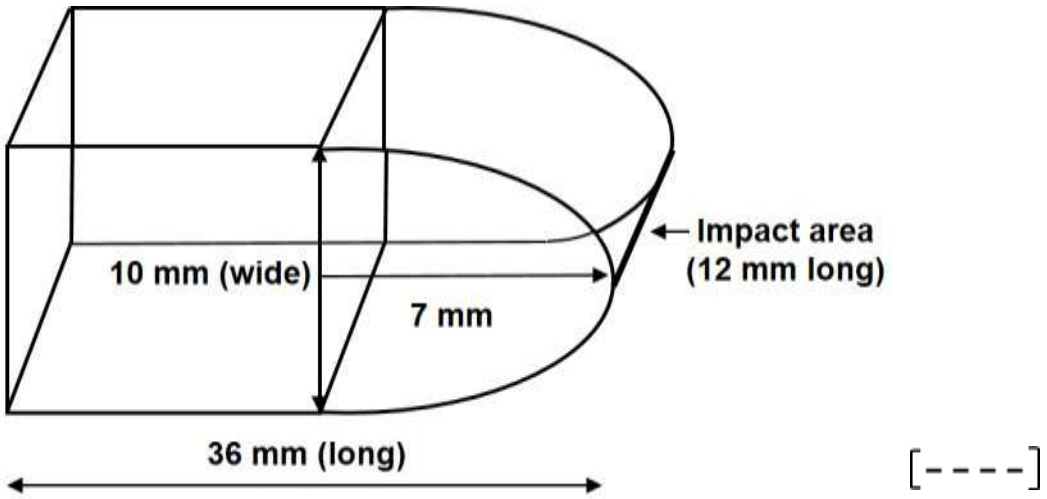

Fig. 9: Schematic illustration of the mid-diaphysis cross section with anterior and posterior impact. Note the large contact area in case of posterior impact and the small contact area in case of anterior [- - - -] impact. Local stresses are denoted by black arrows.

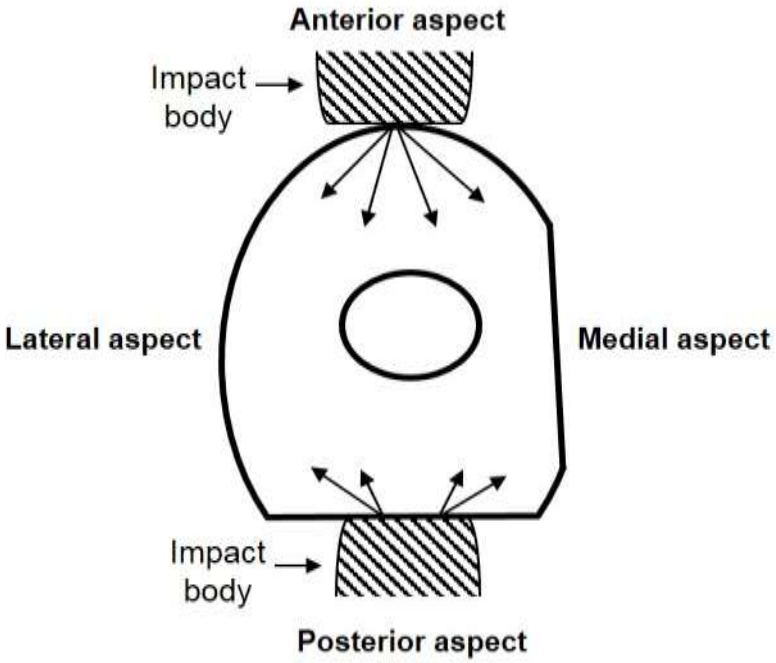

Fig. 10: Schematic illustration of the fracture pattern following lateral impact with axial (compression) loading. Note the large missing fragment, the four oblique lines (**POA =** proximal oblique anterior, **POP** = proximal oblique posterior) (**DOA =** distal oblique anterior, **DOP** = distal oblique posterior) (long dashed lines =). These oblique lines run posteriorly and anteriorly, eventually forming two polygons. Note the incomplete T line on the impact and anterior aspect, the CL-

longitudinal lines, and the short radiating lines running from the oblique lines on the anterior aspect (short dashed lines=).

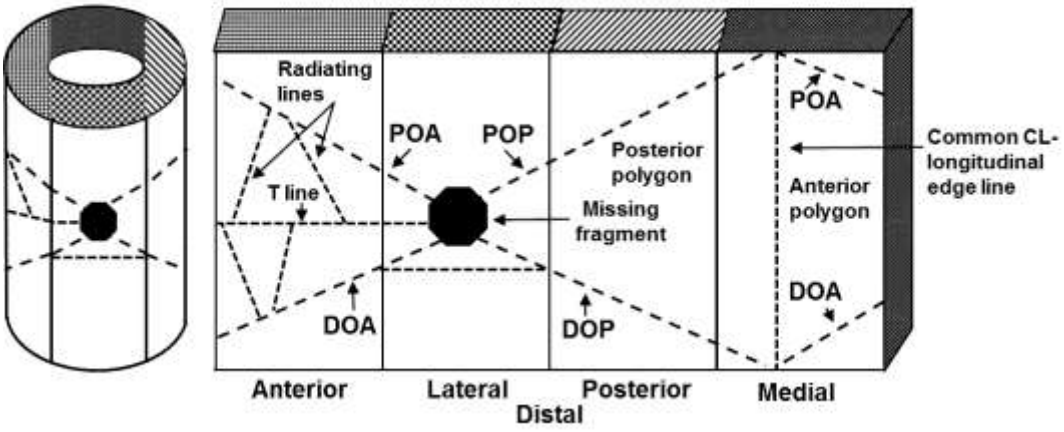

Table 1: Fracture metrical characteristics under different impact directions

Measurements	Direction of impact								
	Lateral impact Test 1 (T_1)		**Posterior impact Test 2 (T_2)**		**Medial impact Test 3 (T_3)**		**Anterior impact Test 4 (T4)**		**P value***
	Mean	**+SD**	**Mean**	**+SD**	**Mean**	**+SD**	**Mean**	**+SD**	
Bone length (mm)	202.0	10.3	197.7	9.6	198.7	9.1	198.7	13.1	0.800 **A**
Cross-sectional moment of inertia (mm^4)	12542.2	1765.9	12788.5	2182.1	14558.4	3781.3	11467.8	2223	0.060 **A**
Number of fracture lines	4.5	1.3	2.9	1.7	3.8	1.3	3.6	0.9	**T_1 vs. T_2 K**
Fracture line/polygo length (mm)	265.7	127.7	165.7	92.8	177.8	123.6	176.6	71.5	0.140 **A**
Chip size (mm)	33.5	13.8	0	0	33.9	16.3	48.9	7.7	0.074 **T**

***Statistically significant at p<0.05 (marked in bold)**
K - Kruskal-Wallis test
A - One-way ANOVA test
T - T-test

Table 2: Presence of fracture features in different impact directions

Measurements	Direction of impact								
	Lateral impact Test 1 (T_1)		Posterior impact Test 2 (T_2)		Medial impact Test 3 (T_3)		Anterior impact Test 4 (T4)		P value Chi-square*
	Present	Absent	Present	Absent	Present	Absent	Present	Absent	
Longitudinal lines	9	1	3	7	7	3	7	3	**0.039**
Polygon	9	1	4	6	4	6	6	4	0.07
Chip fragment	5	5	0	0	3	7	7	3	**0.01**

*** Statistically significant at P<0.05 (marked in bold)**

Table 3: Distribution of the location of longitudinal lines by impact direction (N=10 in each group)

	Location of longitudinal lines (aspect)			
Impact direction	**Impact**	**Contra lateral**	**Impact + contra**	**Anterior**
Lateral impact (Test 1)	25%	50%	0	25%
Posterior impact (Test 2)	34%	0	66%	0
Medial impact (Test 3)	57.5%	14%	28.5%	0
Anterior impact (Test 4)	72%	14%	14%	0

Table 4: The average number of fracture lines by the impact direction

Bone aspect / Impact direction	Lateral		Anterior		Posterior		Medial		P* value
	Mean	Std.	Mean	Std.	Mean	Std.	Mean	Std.	
Lateral impact	4.3	1.2	2.5	0.7	2.2	0.6	2.7	0.9	**0.001**
Anterior impact	1.8	0.8	4.2	0.8	1.9	0.6	2	0.7	**<.001**
Medial impact	2.3	0.7	2	0.7	1.3	0.5	2.9	1.5	**0.004**
Posterior impact	1.4	0.52	2.4	1.1	2	1	1.3	0.5	0.05

***Kruskal-Wallis test**
Statistically significant at p<0.05 (marked in bold)

Table 5: Fracture metrical characteristics with and without axial loading

Measurements	Test 5 (With axial loading)		Test 1 (Without axial loading)		P value*
	Mean	+SD	Mean	+SD	
Bone length	199.1	12.3	202.0	10.3	0.780 **T**
Cross-sectional moment of inertia (mm^4)	14518.8	4563.3	12542.2	1766.0	0.200 **T**
Number of fracture lines	6.1	1.7	4.5	1.3	**0.030 T**
Fracture line/polygon length (mm)	306.1	121.8	265.7	127.7	0.470 **T**
Chip size (mm)	75.1	19.8	33.5	13.8	**0.002 T**
Number of longitudinal lines	0	0	1.3	0.7	**<0.01 M**

*** Statistically significant at p<0.05 (marked in bold)**
T - T-test
M- Mann-Whitney test

Table 6: The average number of fracture lines by bone aspect and the presence of axial loading (tests 1 & 5): lateral impact

Bone aspect / Loading	Lateral		Anterior		Posterior		Medial		P* value
	Mean	**Std.**	**Mean**	**Std.**	**Mean**	**Std.**	**Mean**	**Std.**	
With axial loading	4.9	1.8	3.6	1.4	3.2	1.8	3.3	1.6	0.120
Without axial loading	4.3	1.2	2.5	0.7	2.2	0.6	2.7	0.9	**0.001**

***Kruskal-Wallis test**
Statistically significant at p<0.05 (marked in bold)